

DYNAMICAL EVIDENCE FOR A MAGNETOCENTRIFUGAL WIND FROM A 20 M_{\odot} BINARY YOUNG STELLAR OBJECT

L. J. GREENHILL,¹ C. GODDI,² C. J. CHANDLER,³ L. D. MATTHEWS,⁴ AND E. M. L. HUMPHREYS²

Draft version June 5, 2018

ABSTRACT

In Orion BN/KL, proper motions of $\lambda 7$ mm vibrationally-excited SiO masers trace rotation of a nearly edge-on disk and a bipolar wide-angle outflow 10-100 AU from radio Source I, a binary young stellar object (YSO) of $\sim 20 M_{\odot}$. Here we map ground-state $\lambda 7$ mm SiO emission with the Very Large Array and track proper motions over 9 years. The innermost and strongest emission lies in two extended arcs bracketing Source I. The proper motions trace a northeast-southwest bipolar outflow 100-1000 AU from Source I with a median 3D motion of $\sim 18 \text{ km s}^{-1}$. An overlying distribution of $\lambda 1.3$ cm H₂O masers betrays similar flow characteristics. Gas dynamics and emission morphology traced by the masers suggest the presence of a magnetocentrifugal disk-wind. Reinforcing evidence lies in the colinearity of the flow, apparent rotation across the flow parallel to the disk rotation, and recollimation that narrows the flow opening angle ~ 120 AU downstream. The arcs of ground-state SiO emission may mark the transition point to a shocked super-Alfvénic outflow.

Subject headings: ISM: individual objects (Orion BN/KL) — ISM: jets and outflows — ISM: Kinematics and dynamics — ISM: molecules — masers — stars: formation

1. INTRODUCTION

The balance of gravitational, radiative, and magnetic forces driving high-mass star formation is poorly understood, in part because it has not been possible in general to resolve regions where outflows are launched and collimated. Complicating study, high-mass young stellar objects (YSOs) are deeply embedded during the accretion phase, evolve rapidly, and tend to form in distant crowded regions for which observations may be confusion-limited.

The nearest high-mass YSO, radio Source I in Orion BN/KL (418 ± 6 pc; Kim et al. 2008) offers unique opportunities for investigation. It is deeply embedded (Greenhill et al. 2004a) in a crowded region (Gezari et al. 1998; Shuping et al. 2004). However, it is surrounded by a compact ionized disk with $R \sim 40$ AU resolved in the radio continuum (Goddi et al. 2011a), interpreted as either a hypercompact-HII region at $T \sim 8000$ K emitting p/e Bremsstrahlung around a $\sim 10 M_{\odot}$ YSO or a massive disk at $T < 4500$ K emitting via H⁻ opacity and heated by $\sim 10^5 L_{\odot}$ (Reid et al. 2007; Plambeck et al. 2013). Goddi et al. (2011a) have estimated a robust dynamical mass of $\sim 20 M_{\odot}$ in an equal-mass binary, favoring p/e Bremsstrahlung.

Gas dynamical study is enabled by an unusually large number of maser transitions of SiO and H₂O excited by the YSO (e.g., Goddi et al. 2009; Greenhill et al. 1998). Specifically, the position-velocity structure of vibrationally-excited SiO masers at projected radii of 10–100 AU, resolved with very long baseline interferometry, outlines the limbs of a nearly edge-on, ~ 14 AU thick ob-

scuring disk and a bipolar wide-angle outflow oriented northeast-southwest (Greenhill et al. 2004b; Kim et al. 2008; Matthews et al. 2010). Maser proper motions clearly trace rotation and expansion in a disk/outflow (Matthews et al. 2010).

Here, we analyze angular distributions and time evolution for ground-state $\lambda 7$ mm SiO and $\lambda 1$ cm H₂O maser emission around Source I. The masers sample outflow on scales up to 1000 AU, reinforcing the disk-outflow model, and provide among the best dynamical evidence thus far of a magnetocentrifugal disk-wind (Blandford & Payne 1982; Königl & Pudritz 2000) associated with a high-mass YSO.

2. OBSERVATIONS

We observed SiO and H₂O maser emission toward Source I with the Very Large Array (VLA) of the National Radio Astronomy Observatory⁵ at multiple epochs over 9 years (Table 1).

SiO— We correlated two simultaneous, single-polarization basebands per epoch, one tuned to the $v=0$ transition ($\nu_{\text{rest}} = 43423.79$ MHz) and the other to the much stronger $v=1$ transition ($\nu_{\text{rest}} = 43122.08$ MHz). 3C286 or 3C48 were used as absolute flux calibrators; 0530+135 or 3C84 were used as bandpass calibrators. A 6.25 MHz bandwidth covered $V_{\text{lsr}} = -13.7$ to 29.4 km s^{-1} toward Source I, with 97.656 kHz (0.65 km s^{-1}) channel spacing.

We selected a strong $v=1$ Doppler component as a reference to self-calibrate antenna gain and tropospheric fluctuations on 10^8 time-scales. Scans of J0541–056 enabled calibration of slowly-varying phase offsets between the signal paths for the two observing bands every 15–30^m, which enabled us to transfer the antenna and tropospheric calibration to the band containing the (weaker)

¹ Harvard-Smithsonian Center for Astrophysics, 60 Garden Street, Cambridge, MA 02138 USA; greenhill@cfa.harvard.edu.

² European Southern Observatory, Karl-Schwarzschild-Strasse 2 D-85748 Garching bei München, Germany

³ NRAO, P.O. Box O, Socorro, NM 87801

⁴ MIT Haystack Observatory, Off Route 40, Westford, MA 01886

⁵ The NRAO is a facility of the National Science Foundation operated under cooperative agreement by Associated Universities, Inc.

Table 1
Summary of Observations

Date (yyymmdd)	Project	Array ^(a)	Beam (mas) (°)	RMS (mJy)
²⁸ SiO $J = 1 \rightarrow 0$ $v=0, 1$				
1999.08.28	AG 575	A+	61×43 @ $+44^\circ$	10-40
2002.03.31	AG 622	A+	55×45 @ -31°	6-20
2006.04.15	AC 817	A+	53×39 @ -3.8°	2.5-8.5
2009.01.12	AG 815	A	53×43 @ $+3.6^\circ$	3-20
$\text{H}_2\text{O } 6_{16} - 5_{23}$				
2001.01.23	AG 578	A+	113×48 @ $+30^\circ$	> 6

(a) A: 35 km maximum baseline; A+: 73 km maximum baseline via addition of the Pie-Town antenna.

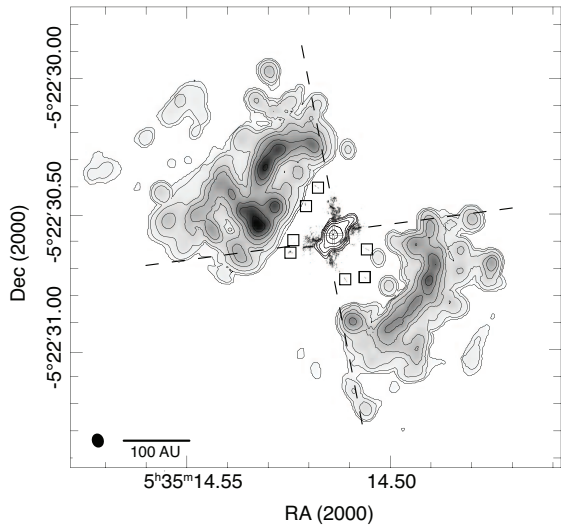


Figure 1. Nested tracers of gas surrounding Source I as observed at $\lambda 7$ mm. Velocity-integrated emission from the $v=0$ $J = 1 \rightarrow 0$ transition of SiO (this work; epoch 2002.25) is shown in grayscale ($26 \text{ Jy } \text{bm}^{-1} \text{ km s}^{-1}$ peak) with overlaid logarithmic contours (2^N). Compact contours at the center depict $\lambda 7$ mm continuum emission (Goddi et al. 2011a). Black “fuzz” extending beyond these contours depicts the distribution SiO $v=1,2$ maser emission as imaged with the VLBA (Matthews et al. 2010). The bulk of this emission lies in densely-sampled loci (“arms”) within ~ 50 AU of Source I, but isolated clumps (outlined in boxes for clarity) are found out to ~ 80 AU. Dashed lines extend the four SiO $v=1,2$ arms to highlight that the $v=0$ emission subtends the same opening angle as structures on smaller scales.

$v=0$ line (see Goddi et al. 2009).

We imaged a region within $\pm 5''$ of Source I. Because $v=0$ emission contains both extended and compact maser components ($T_b^{\text{peak}} \sim 4 \times 10^6 \text{ K}$), we used uniform (u, v) weighting to isolate compact knots and estimate proper motions. For other purposes, we used ROBUST=0 weighting in AIPS (Table 1).

We tracked proper motions for 457 maser spots for between 2 and 4 epochs. To estimate proper motions, we searched for maser spots stronger than 5σ within each channel-map and fit each with a two-dimensional elliptical Gaussian to obtain position, flux-density, and angular size. Images of $v=0$ emission are noise-limited, and relative position errors are given by $0.5 \frac{\theta}{\text{SNR}}$, where θ is beamwidth and SNR is the peak intensity divided by the RMS noise in each velocity channel. Uncertainties for moderately bright emission were a few mas. Cross-referencing of maser spots among different epochs could

be done by eye because the structure of the emission in each channel persisted with shifts of < 1 beamwidth. Proper motions were calculated using an error-weighted linear least-squares fit to the fitted positions. To correct for motion of the reference $v=1$ component, we computed proper motions relative to the strong $v=0$ feature at $+2.7 \text{ km s}^{-1}$ and then subtracted the mean motion of all those measured ($6.11 \pm 0.02 \text{ km s}^{-1}$ in right-ascension, $23.26 \pm 0.04 \text{ km s}^{-1}$ in declination).

We inferred absolute astrometry by measuring separation from BN, in frequency-averaged images. This agreed with that obtained using fast-switching to J0541-0541. The estimated absolute position uncertainty is ~ 3 mas, (based on this comparison).

H₂O— We correlated pairs of overlapping basebands, stepped to cover $V_{\text{lsr}} = -138$ to 137 km s^{-1} ($\nu_{\text{rest}} = 22235.08 \text{ MHz}$). We report here on mapping features in the so-called H₂O Shell (Genzel et al. 1981) associated with Source I. Each baseband was 1.56 MHz and channel spacing was 0.16 km s^{-1} after Hanning-smoothing. 3C286 and J0530+135 were observed as absolute-flux and bandpass calibrators, respectively. One band within each pair was tuned to include the line emission peak near -4.5 km s^{-1} . Ringing affected the strongest emission between -4.02 and -5.18 km s^{-1} . We flagged these data and used the emission at -3.86 km s^{-1} (1700 Jy) to obtain self-calibration solutions every 10^8 that were applied to both 1.56 MHz bands. Scans of J0541-056 every 45^m enabled calibration of instrumental phase offsets between bands. We detected emission from -10.0 to 16.4 km s^{-1} , complete to $\sim 1 \text{ Jy}$ in each channel, except between 8.5 and 11.3 km s^{-1} where the completeness limit was restricted to 2–8 Jy due to dynamic range.

Absolute astrometry was derived from interleaved scans of water maser emission and J0605-085, calibrated using J0541-0541, all observed in dual-polarization continuum mode with 25 MHz bandwidth. The estimated absolute position uncertainty is 2 mas.

3. RESULTS

The most intense $v=0$ SiO maser emission occupies two arcs bracketing Source I, each at a projected radius of ~ 100 AU. This is just outside the maximum radius at which isolated $v=1$ masers are observed (Figure 1). The arcs subtend about the same opening-angle as the nearly radial arms at smaller radii, along which $v=1,2$ maser features are seen to move systematically outward (Matthews et al. 2010). The northeast arc also overlies in part a $3.78 \mu\text{m}/4.67 \mu\text{m}$ color temperature minimum (Sitarski et al. 2013).

The angular structure of the $v=0$ emission is suggestive of outflow in the sky-plane, and its velocity structure confirms it (Figure 2). We tracked proper motions of 59 maser spots for four epochs, 169 for three epochs, and 219 for two epochs (457 total). The median proper motion for maser spots tracked for at least 3 epochs was 18 km s^{-1} . The corresponding range of 3D velocities in the local frame ($V_{\text{LSR}}=5 \text{ km s}^{-1}$) was $4\text{--}36 \text{ km s}^{-1}$. Overlap in the ranges of radial velocity for the two lobes suggests a close to edge-on geometry (Figure 2, upper-left panel). Interpretation as an outflow is strengthened by H₂O maser emission overlying each lobe of $v=0$ SiO emission (Figure 2). The H₂O emission displays a similar range of line-of-sight velocity (-10.0 to 16.4 km s^{-1}).

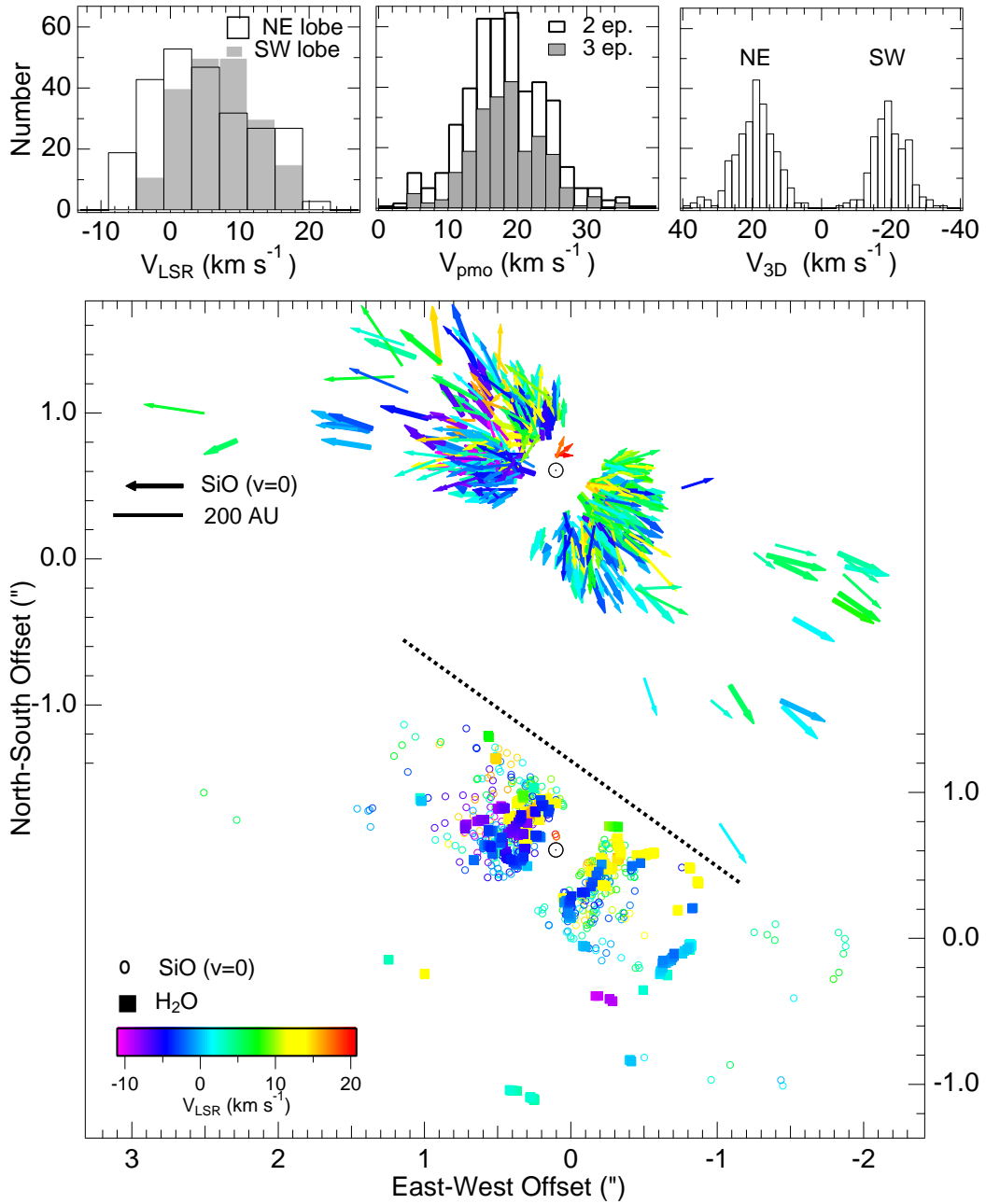


Figure 2. Tracers of outflow at radii of 10–1000 AU from Source I. (*bottom*) Overlay of SiO $v=0$ (*circles*) and H₂O masers (*squares*); the latter appear more concentrated toward Source I (\odot) (*middle*) Proper motions for SiO $v=0$ emission clumps, 1999 to 2009. Proper motions of SiO $v=0$ emission centroids tracked over 3 or 4 epochs (heavy arrows) and for 2 epochs (light arrows). The horizontal black arrow indicates motion of 30 km s⁻¹. On both halves of the lower panel, colors indicate V_{LSR} in km s⁻¹ (*color bar*); the systemic velocity is 5 km s⁻¹. (*upper left*) Distributions of line-of-sight velocities of SiO masers in the northeast and southwest lobes; their similarity indicates a flow-axis close to the sky-plane. (*upper middle*) Histogram of proper motions of SiO spots measured over at least three epochs (*shaded*) or two epochs (*unshaded*). (*upper right*) Distributions of total space velocity for SiO maser spots in the northeast and southwest lobes.

A 20 km s^{-1} expansion in the angular extent of the H_2O distribution over ~ 8 years (Greenhill et al. 1998) and ~ 18 years (Figure 4, lower-left panel) is consistent with the median SiO maser proper motion.

The flow orientation can be estimated from the emission locus as well as the sky position and proper motions of maser spots. We obtain a common mean position angle (PA) of 56° by reflecting the southwest lobe about a northwest-southeast line at PA 142° , which minimizes the standard deviation of the overlapping distributions (29°). Using the most reliable proper motions (derived from ≥ 3 epochs), the mean motion lies at a PA = $55 \pm 34^\circ$ (northeast) and $-128 \pm 43^\circ$ (southwest). Reflecting the southwest lobe, we obtain a mean outflow PA = 55° and a minimum standard deviation of 34° for a reflection axis of 142° . Hence, we take $56 \pm 1^\circ$ as the PA of the outflow, measured independently from emission locus and proper motions.

Although the flow inside $\sim 100 \text{ AU}$ appears to follow a fixed opening-angle, the outflow further downstream appears to become more narrowly collimated. Indeed, the inner quartile range of maser motion position angles at projected radii $0''.1\text{--}0''.3$ from Source I is 80° , broader than the range of 47° beyond $0''.3$ (120 AU).

From our measurements, we estimate the outflow mass-loss rate $\dot{M} = 5 \times 10^{-6} V_{18} R_{200}^2 n_6 \Omega / 4\pi M_\odot \text{ yr}^{-1}$, where V_{18} is the average maser velocity in units of 18 km s^{-1} , R_{200} is the average distance of SiO masers in units of 200 AU , n_6 is the volume density in units of 10^6 cm^{-3} , and Ω is the solid angle for a conical flow. The main uncertainty in the formula above is the density required for excitation of ground-state SiO masers, known within an order of magnitude ($10^{6 \pm 1} \text{ cm}^{-3}$; Goddi et al. 2009).

There is no indication of acceleration/deceleration with radius in the flow. But interestingly, in each lobe there is a discernible velocity offset across the minor axis, manifested in the line-of-sight velocities of both SiO and H_2O masers (e.g., Figure 3, upper panel). Toward the southeast-facing edge, there is a greater preponderance of blueshifted emission; redshifted emission lies preferentially toward the northwest. The velocity data exhibit a non-Gaussian scatter, so to quantify the trend, we estimate the trimean LSR velocity (the weighted average of median and quartiles) as a function of distance along the minor axis for emission $0''.1\text{--}0''.4$ from Source I: a 5 km s^{-1} shift for $v=0$ SiO and a 10 km s^{-1} shift for H_2O maser emission. We interpret this velocity offset as a signature of rotation parallel to the minor axis of the flow.

Ground state SiO $J = 1 - 0$ maser emission and proper motions displayed in Figures 1-3 trace only the inner portions of the bipolar outflow traced by $J = 2 - 1$ emission and mapped with CARMA at $0''.5$ resolution (Plambeck et al. 2009), or the $J = 5 - 4$ emission mapped with ALMA at $1''.5$ resolution (Zapata et al. 2012; Niederhofer et al. 2012). These transitions show basically the same “butterfly” morphology at projected radii $\lesssim 500 \text{ AU}$ and excellent agreement in the outflow PA (56°). While complex brightness and velocity-field morphologies are evident well away from Source I, this may be a consequence of external heating (Niederhofer et al. 2012), e.g., by the Hot-Core and compact mid-infrared sources (Figure 4).

4. DISCUSSION

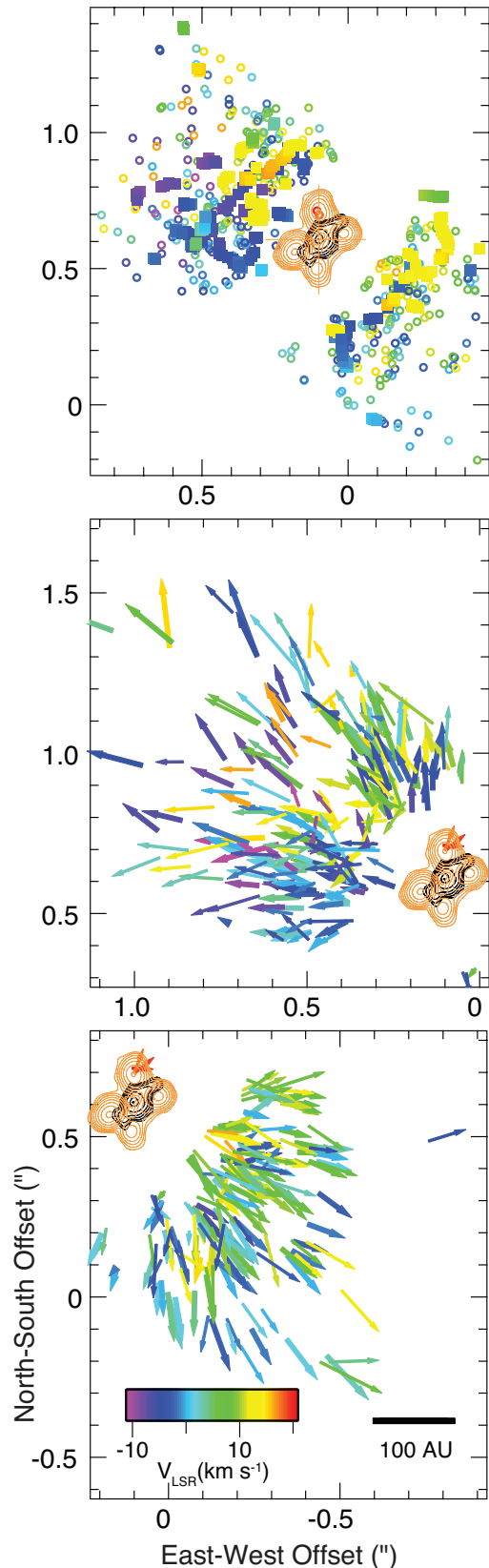


Figure 3. Expanded view of the outflow. (*top*) SiO $v=0$ and H_2O masers (*open circles and squares*, respectively), velocity-integrated SiO $v=1$ masers (*red contours*), and Source I $\lambda 7 \text{ mm}$ continuum (*black contours*), as mapped with the VLA. (*middle*) Expanded view of SiO $v=0$ maser proper motions in the northeast lobe of Source I. (*bottom*) Expanded view of the southwest lobe.

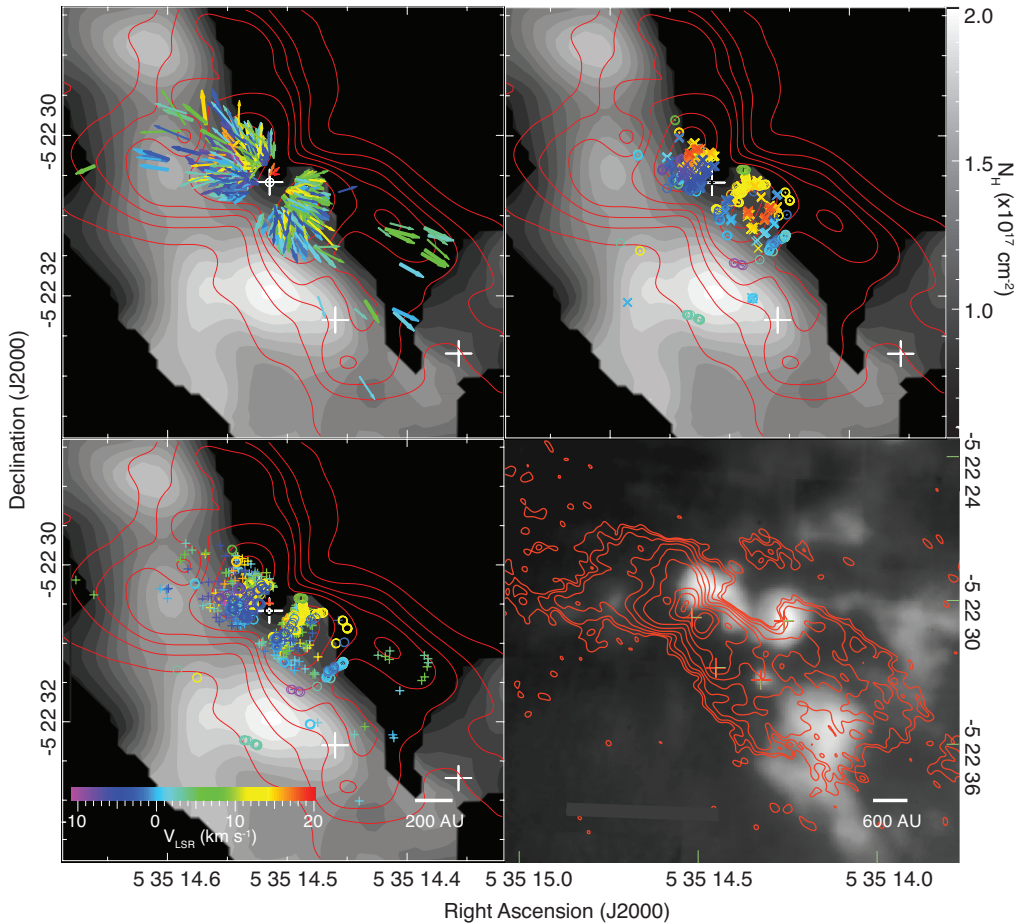


Figure 4. Source I outflow, dense Hot-Core gas, and proximate mid-infrared sources. The outflow is shown in velocity-integrated emission of $\lambda 3\text{ mm } J = 2 \rightarrow 1$ emission covering -5 to 5 km s^{-1} , observed with a beamwidth of $0''.5$ (red contours; Plambeck et al. 2009). Contours are 3.5, 1.9, 0.55, 0.30, 0.16, 0.086, 0.046, 0.025 Jy bm^{-1} averaged over 10 km s^{-1} . Only the lower right panel includes the lowest two levels. Dense gas is shown via an NH_3 column-density map with $0''.8$ beamwidth (greyscale; Goddi et al. 2011b). The lower-right panel substitutes a mid-infrared image obtained with Keck (Greenhill et al. 2004a). Crosses mark the positions of three YSOs: sources I, SMA1, and n (left to right, as in Goddi et al. 2011b). (Upper-left) Proper motions of outflowing SiO $v=0$ masers (arrows). (Upper-right) Superposition of H_2O masers observed in 1983 (\times) - Greenhill et al. (1998), and 2001 (\circ) - this work, demonstrating expansion of the locus. (Lower-left) Superposition of SiO $v=0$ ($+$) and H_2O masers in 2001 (\circ). (Lower-right) Overlay of the SiO outflow with mid-infrared sources over a larger field-of-view.

4.1. Outflow 100–1000 AU from Source I

The X-shaped morphology traced by vibrationally-excited SiO maser emission within 100 AU of Source I is interpreted as the edges of a bipolar outflow orthogonal to an edge-on rotating disk (Matthews et al. 2010). Our new mapping of the ground-state SiO and H_2O maser emission confirms and extends to 1000 AU the disk-outflow model. Three lines of evidence support this scenario: (i) the most intense $v=0$ SiO maser emission occupies two arcs that bracket Source I at a radius of ~ 100 AU and subtend an angle corresponding to the opening-angle of the vibrationally-excited SiO masers; (ii) the PA of the outflow at radii >100 AU is the same as that of the disk and flow axes at small radii; (iii) the line-of-sight velocities of $v = 0$ SiO masers indicate an outflow close to the sky-plane, consistent with the nearly edge-on disk.

Three striking features in the outflow are evident from our measurements: colinearity, recollimation, and rotation.

Colinearity of northeast and southwest flows (§3) is notable because (i) Source I lies at the edge of the

dense gas associated with the Orion Hot-Core (Figure 4; Goddi et al. 2011b), (ii) the outflow motion is comparable to the stellar motion, (iii) SiO maser dynamics inside 1000 AU are indicative of a ~ 500 yr crossing time for the outflow, and (iv) the crossing time for Source I from the center of dynamical interaction with BN is also ~ 500 yr (Goddi et al. 2011a), indicating that the onset of flow is contemporaneous with the interaction with BN. For a hypothetical hydrodynamic flow, the absence of curvature as a result of the YSO motion requires the momentum flux to exceed that of the ambient medium into which Source I is moving. Since ground-state SiO maser emission requires densities of 10^6 - 10^7 cm^{-3} (e.g., Goddi et al. 2009), the density of ambient material would have to be $\ll 10^6\text{ cm}^{-3}$. However, ambient gas densities in the vicinity of the Hot-Core are at least this (e.g., Goddi et al. 2011b), thus requiring greater flow energy density than from hydrodynamics alone.

Outflow (re)collimation is indicated by a narrower distribution of SiO proper motion position angles far from the YSO, as well as greater preponderance of line-of-sight velocities close to systemic (§3; Figures 2, 3). Mechanical collimation from the ambient medium is rendered prob-

lematic by the similarity of the leading and trailing edges of the flow despite the anticipated ambient density gradient toward the Hot-Core. In principle, maser excitation effects could bias the inferred morphology of the flow if these favor emission close to the outflow axis, but this would not explain comparable leading and trailing edge gradients in the intensity of thermal SiO emission (e.g., Figure 4, top).

Finally, there is a discernible rotation signature about the major axis of the flow in each lobe, consistent with the rotation observed at radii of tens of AU in the vibrationally-excited SiO masers (Matthews et al. 2010). Our data are suggestive of these dynamics being communicated from scales of $O(10)$ AU to at least $O(100)$ AU.

4.2. Magnetocentrifugal Wind from a high-mass YSO

The possibility of a magnetohydrodynamic disk-wind is raised by the evidence of a rotating wide-angle outflow launched from a compact disk, that is recollimated downstream, and that proceeds undeflected through a dense medium. Rotation is anticipated for a magnetized outflow with the field anchored to a rotating disk. Magnetic field lines threading the flow would raise its energy density, while a toroidal field and corresponding hoop stress generated by rotation could efficiently narrow collimation with distance.

Matthews et al. (2010) conservatively interpreted the maser data in the context of Keplerian motion and the dominant action of gravity, inferring a dynamical mass of $\sim 8 M_{\odot}$. However, early indirect evidence of non-gravitational effects were noted (e.g., curved maser trajectories), possibly due to magnetic fields, by which rotation would appear Keplerian though the YSO mass would be underestimated. The latter is consistent with the difference between YSO masses inferred by Matthews et al. (2010) and Goddi et al. (2011a) under the assumption that BN and Source I are in recoil (cf. Chatterjee & Tan 2012). This early evidence, along with the morphology and dynamics of outflow on scales out to 1000 AU, strengthens the case for a magnetic flow.

Using axisymmetric MHD numerical simulations, Vaidya & Goddi (2013) have explored the plausibility of an MHD origin of the wide-angle flow probed by vibrationally-excited SiO masers inside 100 AU from Source I, and proposed that the SiO masers may be excited as an MHD driven wind interacts with the ambient molecular medium in form of shocks. Seifried et al. (2012) studied earlier conditions, applying MHD theory from the collapse of magnetized cloud cores to disk formation and outflow launching, and demonstrated magnetocentrifugal launching of massive outflows, similar to the case of low-mass outflows.

Why do intense ground-state SiO and H₂O maser emission arise suddenly at 100 AU? Why are SiO and H₂O masers apparently intermixed when the densities required for emission differ by (conservatively) an order of magnitude? For a YSO luminosity of $2 \times 10^4 L_{\odot}$ (i.e., a binary with two $10 M_{\odot}$ stars), the sublimation radius is $\ll 100$ AU, and since maser emission requires a high gas-phase abundance, its appearance so far out in the flow is significant.

We propose that the arcs of maser emission at ~ 100 AU radius indicate the onset of strong shocks in dusty outflowing material. Hydromagnetic C-type shocks as

slow as $10\text{-}20 \text{ km s}^{-1}$ (comparable to the flow speed) are capable of sputtering grains (Schilke et al. 1997; Van Loo et al. 2013, and references therein), a process that would raise the gas-phase abundance of SiO and H₂O. Formation of two continuous shock structures subtending broad ranges of polar angle and narrow ranges in radius indicates a systematic change in physical conditions. Transition to a super-Alfvénic flow and consequent shock formation may trigger the observed (re)appearance of maser emission in the outflow at ~ 100 AU. Decline in Alfvén velocity below the outflow velocity would require the magnetic field to decline at least linearly with radius if density falls quadratically. This is not implausible. An observational consequence is that the inner edge of the maser emission locus would not appear to expand with time.

The presence of maser emission well downstream, suggests persistent high gas-phase abundance, as well as energy that can drive maser pumping. Flow speeds in excess of the sound and Alfvén speeds would drive shocks and impart pump energy over a wide range of radii, assuming that cooling timescales are much shorter than dynamical time scales. In this region, observed fading of the velocity gradient indicative of rotation around the flow axis is consistent with decoupling of the neutral gas from the field as expected from MHD disk-wind models.

5. CONCLUSIONS

Data for SiO and H₂O masers provide an unusually detailed view of the launch and collimation of an outflow from the surface of a compact disk surrounding Source I in BN/KL. Position and velocity resolved gas dynamics at projected radii of 10 AU to 1000 AU suggest the presence of a magnetocentrifugal disk-wind driven by a massive YSO. This is notable in view of continuing ambiguity concerning the role of magnetic fields in high-mass star formation. While the outflow structure up to 1000 AU in this high-mass YSO is remarkable in terms of symmetry, colinearity, collimation, and rotation, larger scales reveal the effects of the interaction of the massive outflow with the typically complex environment of a massive star forming region.

REFERENCES

- Blandford, R. D. & Payne, D. G. 1982, MNRAS, 199, 883
 Chatterjee, S., & Tan, J. C. 2012, ApJ, 754, 152
 Genzel, R., Reid, M. J., Moran, J. M., & Downes, D. 1981, ApJ, 244, 884
 Gezari, D. Y., Backman, D. E., & Werner, M. W. 1998, ApJ, 509, 283
 Goddi, C., Greenhill, L. J., Chandler, C. J., Humphreys, E. M. L., Matthews, L. D., & Gray, M. D. 2009, ApJ, 698, 1165
 Goddi, C., Humphreys, E. M. L., Greenhill, L. J., Chandler, C. J., Matthews, L. D. 2011a, ApJ, 728, 15
 Goddi, C., Greenhill, L. J., Humphreys, E. M. L., Chandler, C. J., & Matthews, L. D. 2011b, ApJ, 739, L13
 Greenhill, L. J., Gwinn, C. R., Schwartz, C., Moran, J. M., & Diamond, P. J. 1998, Nature, 396, 650
 Greenhill, L. J., Gezari, D. Y., Danchi, W. C., Najita, J., Monnier, J. D., & Tuthill, P. G. 2004a, ApJ, 605, L57
 Greenhill, L. J., Reid, M. J., Chandler, C. J., Diamond, P. J., & Elitzur, M. 2004b, Star Formation at High Angular Resolution, 221, 155
 Kim, M. K., et al. 2008, PASJ, 60, 991
 Königl, A. & Pudritz, R. E. 2000, Protostars and Planets IV, ed. V. Mannings, A. P. Boss, & S. S. Russell (Tucson, AZ: Univ. Arizona Press), 759

- Matthews, L. D., Greenhill, L. J., Goddi, C., Chandler, C. J., Humphreys, E. M. L., & Kunz, M. 2010, *ApJ*, 708, 80
- Niederhofer, F., Humphreys, E. M. L., & Goddi, C. 2012, *A&A*, 548, A69
- Plambeck, R. L., Wright, M. C. H., Friedel, D. N., et al. 2009, *ApJ*, 704, L25
- Plambeck, R. L., Bolatto, A. D., Carpenter, J. M., et al. 2013, *ApJ*, 765, 40
- Reid, M. J., Menten, K. M., Greenhill, L. J., & Chandler, C. J. 2007, *ApJ*, 664, 950
- Schilke, P., Walmsley, C. M., Pineau des Forets, G., & Flower, D. R. 1997a, *A&A*, 321, 293
- Seifried, D., Pudritz, R. E., Banerjee, R., Duffin, D., & Klessen, R. S. 2012, *MNRAS*, 422, 347
- Shuping, R. Y., Morris, M., & Bally, J. 2004, *AJ*, 128, 363
- Sitarski, B. N., Morris, M. R., Lu, J. R., Duchêne, G., Stolte, A., Becklin, E. E., Ghez, A., Zinnecker, H. 2013, *ApJ*, in press
- Vaidya, B., & Goddi, C. 2013, *MNRAS*, 429, L50
- Van Loo, S., Ashmore, I., Caselli, P., Falle, S. A. E. G., & Hartquist, T. W. 2013, *MNRAS*, 428, 381
- Zapata, L. A., Rodríguez, L. F., Schmid-Burgk, J., et al. 2012, *ApJ*, 754, L17